Selection of Adequate EPS-Block Geofoam for Use in Embankments Subjected to Seismic Loads

Marzieh Khosravi [a,*], David Arellano[b]

[a] *University of Memphis, TN, Memphis, USA*
[b]*Department of Civil Engineering, University of Memphis, TN, Memphis, USA*

Abstract

This study provides a methodology for analyzing the load-bearing capacity and horizontal sliding failure mechanisms that are required to complete a seismic internal stability analysis of EPS-block geofoam embankments. The objective of the seismic analysis procedure is to determine stresses from anticipated earthquakes to select the proper type of EPS that can support the anticipated increase in stress due to dynamic stresses and to evaluate potential horizontal displacements that may occur between rows of EPS blocks during a seismic event. The seismic analysis procedure considers the additional stresses due to rocking of the embankment and the impact of lateral sway and damping on horizontal sliding between rows of EPS blocks. The procedure considers both the 1% and 2% strain criteria for selecting the proper EPS block types to support both dynamic and static stresses. The seismic analysis procedure is demonstrated by analysis of one of the EPS-block geofoam embankments that the Tennessee Department of Transportation is proposing as partial replacement of an existing bridge in Memphis, Tennessee in the USA. The dynamic analysis results indicate that the static and dynamic stresses can exceed the elastic limit stress of proposed geofoam types selected based on only static analysis along the extreme outer corners of the embankment. The

---

[*] Corresponding authors.
Email addresses: msh.khosravi2@gmail.com (M Khosravi), darellan@memphis.edu (D Arellano)
Telephone numbers: (901) 678-3272 (D Arellano)
Postal address: University of Memphis, 104 Engineering Science Bldg., Memphis, TN 38152

study revealed that the 2% criterion provides an economical advantage compared to the 1% criterion. Although the 2% axial strain criterion is based on limited test data, if static and temporary dynamic stresses do exceed the cyclic elastic limit of the EPS, the potential consequence can be that long-term creep strains after the earthquake event may be greater than anticipated resulting in overall settlement of the embankment that can be greater than anticipated. However, the additional deformation and settlement of the embankment would typically not result in catastrophic collapse, which is in general agreement with the 'no-collapse' philosophy for seismic design that has been adopted by many state and federal agencies in the USA. The results of the Memphis EPS embankment also indicated that not including live load vehicle stress in the FLAC analysis and not incorporating a factor of safety for evaluation of seismic dynamic stresses appear to be reasonable seismic analysis approaches based on the AASHTO (2020) specifications.

Keywords: EPS, Geofoam, Embankments, Seismic, FLAC

---

1. Introduction

Expanded polystyrene (EPS)- block geofoam is an extremely lightweight fill material utilized in many geotechnical applications such as roadway and railway embankments, bridge approaches and abutments, structure compensation foundations, slope stabilization, airport runways and taxiways, levees, and behind building walls and earth retaining walls. Lightweight fill is a type of ground modification technology (Schaefer et al. 2017) that involves modification of the earth structure such as a roadway embankment but can also involve alteration of

the site foundation conditions by removal of the existing site soil and replacement with lightweight fill. The primary ground modification function of lightweight fill is to decrease the imposed loads on the existing ground. Furthermore, implementation of these type of material reduce the earth pressure fills behind walls and retaining structures, structural support, as well as compressible inclusion's earth pressures, thermal insulation, and vibration damping.

Lightweight fills that have been utilized in transportation projects include expanded-polystyrene (EPS)-block geofoam; cellular concrete; wood fiber; blast furnace slag; boiler slag; fly ash; shredded tires; foamed glass aggregate; expanded shale, clay & slate; pumice; and basalt. Lightweight fills such as EPS-block geofoam have been utilized in transportation projects because it can contribute to cost savings because of the accelerated construction benefit that geofoam provides compared to other ground modification technologies. The comprehensive design guidelines for the use of geofoam in stand-alone embankments is provided by Stark et al. (2004a, 2004b) and for us in slope stabilization is provided by Arellano et al. (2011). One design aspect that has been evolving is the seismic design. The overall design process is divided into three phases: design for external (global) stability of the overall embankment, design for internal stability within the embankment mass, and design of an appropriate pavement system for the subgrade provided by the underlying EPS blocks. The focus of the study presented herein is internal stability.

The primary objective during internal stability is the proper selection and specification of geofoam properties so that the geofoam blocks can provide adequate bearing capacity and support the applied stresses from gravity, traffic,

water, seismic, wind and other loads without excessive immediate and time-dependent compression that can lead to excessive settlement of the pavement surface or surface of the embankment. This primary objective is accomplished by selecting an EPS type that has an elastic limit stress that is greater than the stresses imposed on the EPS from applied loads. The elastic limit stress of EPS is the compressive resistance at 1% strain. Arellano and Stark (2009) provide an overview of the load bearing analysis procedure of geofoam embankments. However, a recent study by Bartlett and Neupane (2017), suggests that for the design of EPS bridge support systems for temporary seismic loads, EPS with a compressive resistance measured at 2% axial strain, which is approximately equivalent to 85 percent of the compressive resistance at 10 percent strain, can be used, provided the EPS blocks have a stress-strain behavior similar to EPS 25. The study herein provides a comparison of the 1% and 2% strain criteria.

Seismic loading is a short-term event that can affect both external and internal stability and, therefore, must be considered in the design of geofoam embankments. Two failure mechanisms that involve seismic internal stability of EPS-block geofoam embankments include load-bearing failure of the EPS blocks and horizontal sliding between blocks (Arellano et al. 2011a; 2011b).

Rocking of the geofoam embankment due to seismic-inertia forces contributes to the vertical stresses on the EPS blocks (Horvath 2011, Horvath 2004,). The impact of the rocking stresses is greatest near the bottom and exterior edges of the embankment. Bartlett and Lawton (2008) recommended installing higher strength geofoam blocks in these general locations to minimize the potential of overstressing the EPS blocks. A seismic study using numerical analysis can consider the additional rocking stresses

during seismic internal stability analysis to obtain the estimated overall stresses within the EPS blocks.

For situations in which EPS-block geofoam is used as a lightweight fill and placed beneath a pavement structure, the pavement system comprises the vast majority of the overall lightweight system's mass, resulting in a structure that is extremely top-heavy. Thus, when a cyclic lateral load is applied, such as that produced by an earthquake, the fill mass structure has a tendency to sway laterally because the ground motion experienced by the foundation soil can be amplified at certain frequencies to such a degree that the EPS-block fill and the pavement system it supports may actually "feel" a vibration of much greater amplitude than that "felt" by the soil immediately beneath it (Horvath 2012, Riad and Horvath, 2004). Therefore, the swaying motion from amplification can contribute to increased horizontal sliding of the EPS blocks near the top of the embankment. However, damping within the EPS fill mass possibly due to energy losses within the assemblage of blocks as well as inter-block sliding friction along joints (Horvath 1995) can also impact the potential for horizontal sliding. A seismic study using numerical analysis can consider the impact of lateral sway and damping on horizontal sliding between rows of EPS blocks.

In summary, two failure mechanisms that involve seismic internal stability of EPS-block geofoam embankments include load-bearing failure of the EPS blocks and horizontal sliding between blocks. Therefore, the two key objectives of a seismic stability analysis are to determine stresses from anticipated earthquakes to select the proper type of EPS that can support the anticipated increase in stress due to dynamic stresses and to evaluate potential horizontal displacements that may occur between rows of EPS blocks during a seismic event. Seismic studies using numerical analysis can

assist with accomplishing both objectives. A seismic study using numerical analysis can also consider the additional rocking stresses to obtain the estimated overall stresses within the EPS blocks and the impact of lateral sway and damping on horizontal sliding between rows of EPS blocks.

Bartlett and Lawton (2008) performed a numerical analysis of a stand-alone EPS-block geofoam stand-alone and modeled the behavior of the embankment under seismic loads generated during a M7.0 earthquake. The analysis was performed using the finite difference program FLAC. Some key conclusions included (1) Interlayer sliding displacement is a highly nonlinear process and is influenced by the frequency content and long period displacement pulses present in the input time histories; (2) For cases where interlayer sliding is just initiating, the vertical component of acceleration is important because an analysis based on only the horizontal component of acceleration may yield unconservative results. However, the vertical component of motion is less important when the interlayer sliding is well developed; and (3) Horizontal sway and rigid-body rocking can cause local tensile and compressive yielding of blocks near the base of the embankment. In several cases, the tensile yielding may propagate upwards and may result in decoupling of the EPS blocks and load distribution slab.

Amini (2014) and Hu et al. (2019) investigated the dynamic characteristics and seismic stability of EPS embankments. Amini applied a harmonic sinusoidal wave and considered interlayer sliding, the fundamental period, and the approximate location of potential yielding EPS blocks. She recommended consideration of higher density geofoam blocks in zones susceptible to overstressing near the basal edges of the embankment.

Although, a comprehensive design guideline for expanded polystyrene block geofoam in static load provided by Arellano et al. (2010), the dynamic load and seismic analysis need to be guided by updated procedures. The study presented herein contributes to the continual evolution of seismic design of geofoam roadway embankments. The primary objective of the study presented in this paper is to provide a process for performing numerical seismic analysis of EPS block embankments with step-by-step guided information. This conclusion of this research considers the result of having both the 1% and 2% strain criteria for selecting the EPS block types and that considers the impact of estimated horizontal displacements. The seismic analysis procedure is demonstrated by analysis of one of the geofoam embankments that the Tennessee Department of Transportation (TDOT) is proposing as partial replacement of an existing 478 m length bridge along Poplar Avenue in Memphis, Tennessee located in the mid-southern part of the United States of America (USA)

2. Background

TDOT is proposing to include two EPS embankments as part of an overall project that involves replacing an existing 478 m length bridge. The seismic analysis of this study includes one of the EPS embankments at Station 25+33.05 that will be 35 m in length, 33 m in width, and 13 m in height. A summary of vertical stresses and horizontal displacements obtained from a seismic analysis of this embankment using the finite difference software program FLAC 2D developed by Itasca Consulting Group (version 8.1) is provided in this study. The seismic analysis procedure is presented next.

3. Methods and Procedure

3.1. Seismic analysis steps

The procedure for performing numerical seismic analysis of the EPS-block

embankment utilized in this study consists of the following steps: (1) developing the

FLAC numerical model, (2) determining acceleration time histories, and (3)

performing the numerical dynamic analysis. A summary of these steps is provided

next.

3.2. Developing the FLAC Numerical Model

The FLAC model represents the cross section of the middle of the EPS

embankment at Station 25+33.05. Figure 1 provides an overview of the FLAC model

with the horizontal interfaces that are included in the model.

The pavement system is 1 m thick and represents the load distribution slab and the

various pavement section materials. The EPS embankment is 12 m high and 33 m

wide. The soil foundation is 12 m in depth and 99 m wide. Interface 1 is the soil

foundation to EPS interface at the bottom of the embankment, Interfaces 2 through 12

are the interfaces between rows of EPS blocks from the bottom to the top of the EPS

embankment, and Interface 13 is the EPS to pavement system contact interface near

the top of the embankment. The interfaces between layers of blocks are spaced at 1 m

intervals to represent 1 m thick EPS blocks. The dimensions of the model and

properties of each material represented in Table 1 and Table 2, respectively.

Appendix A provides details of the numerical modeling validation as the primarily

stage of EPS blocks modeling and seismic analysis.

To create a horizontal slippage surface between the EPS layers, interface

elements were assigned to each layer, and their properties are shown in Table 3.

Interface 1 is the soil foundation/EPS contact surface, interfaces 2 through 12 are EPS

block horizontal layer contact surfaces (from bottom to top, respectively), and interface 13 is the EPS/Pavement System contact interface. Horizontal movement is allowed along "not glued" interface types and no horizontal movement is allowed along "glued" interfaces. A "glued" interface was used for Interface 1 because the bottom most layer of geofoam base is approximately two feet below the proposed ground surface as indicated in the TDOT Structures and Geofoam plans (2020) and it is assumed that horizontal sliding will not occur. A "glued" interface was also assumed between the pavement system and the upper row of EPS 39 (Interface 13). The interfaces between EPS blocks (Interfaces 2 through 12) are modeled with interface types of "not glued". The interfaces are characterized by the interface friction angle and a spring with a stiffness normal to the interface.

The FLAC dynamic manual ("FLAC | US Minneapolis - Itasca Consulting Group, Inc." version 8.1.) recommends defining the stiffness of these springs from the following Equation:

$$k_n = k_s = 10(\frac{K + \frac{4}{3}G}{\Delta Z_{min}}) \tag{1}$$

where K and G are the bulk and shear modulus, respectively; and ΔZ_{min} is the smallest width of an adjoining zone in the normal direction (the mesh size is 1 m for our model). k_n is the normal stiffness (stress/ displacement) and k_s is the shear stiffness (stress/ displacement). For the case where only slippage and separation are considered, at the interface, the FLAC user's manual recommends that the normal and shear interface stiffness (k_n and k_s, respectively) be set to ten times the stiffness of the neighboring zone. When the material on one side of the interface is much stiffer than the

other, then the equation is applied using the material properties of the softer side. In this case, the deformability of the interface was dominated by the soft side.

3.3. Determining Acceleration Time Histories

The procedure for determining time histories to incorporate in the numerical seismic analysis consists of the following sub steps:

(1) obtaining the target response spectrum, (2) selecting appropriate ground motions, (3) obtaining bedrock surface level and shear wave velocity, (4) determining acceleration time histories at the base of the FLAC model (the deconvolution process). A summary of these sub steps is provided subsequently.

3.3.1. Step 1: Obtaining the target response spectrum

The EPS embankment project is located in Memphis, Tennessee, which is located in the mid-southern United States. The Tennessee Department of Transportation (TDOT) required the EPS embankment to be designed to a 1000-year return period based on the AASHTO LRFD bridge design specifications (AASHTO, 2017). AASHTO recommends earthquake ground motions that have a seven percent probability of exceedance in 75 years. The USGS Earthquake Hazards Program - Unified Hazard Tool (2019) suggested a the dominant earthquake at the project site with magnitude equal to 6.74 (g) and the seismic-source-to-site distance of 47.49 km for an earthquake return period of 1000 years.

The soil profile was determined based on the geotechnical properties obtained from geotechnical report. The SPT N values from the soil boring logs met the AASHTO (YEAR) requirements for Site Classification D and Seismic Category C (or Seismic Zone 3). The target response spectrum was obtained from the USGS website by the

Unified Hazard Tool based on the defined soil type and seismic zone on the actual project's location. Uniform hazard response spectrum and probabilistic seismic hazard deaggregation obtained from USGS website led to obtaining the seismic acceleration coefficients of response spectrum parameters as As = 0.412, S_{Ds} = 0.859, S_{D1} = 0.369.

3.3.2. Step 2: Selecting appropriate ground motions

A suite of earthquake ground motions was obtained from the Pacific Earthquake Engineering Research (PEER) ground motion database based on the USGS site-specific response spectrum. The first seven ground motions were selected from the PEER Center website based on earthquakes that have the lowest value of the Mean Square Error (MSE), compared to the obtained target response spectrum.

A spectral matching procedure was performed on all the seven selected motions by the SeismoMatch software program (Seismosoft 2020) to obtain the scaled the unscaled PEER selected motions.

Table 4 shows the seven selected earthquakes included in the PEER database with a magnitude range of 6.1 (g) to 7.2 (g) and a distance range of 15 km to 65 km. After the spectral matching procedure, motion number 6 was chosen from the seven earthquake motions because it had the maximum acceleration value, which changed from 0.019 g to 0.28 g after spectral matching. Figure 2 illustrates the acceleration-time history of the selected motion. Step 3: Obtaining bedrock surface level and shear wave velocity profile.

The bedrock surface level and shear wave velocity profile is needed for the deconvolution process of Step 4 (next step) to account for changes in motion propagation from the bedrock through the soil the soil layers. Bedrock surface level was obtained from the USGS website, and its Central U.S. Seismic Velocity Model

and the shear wave velocity of the soils was determined by using CUSVM Version 1.3 software based on the Poplar Ave. bridge location. The initial 80 ft from the ground surface shear wave velocity values were replaced by the values from the e geotechnical report of the project. Step 4: Determining acceleration time histories at the base of the FLAC model (the deconvolution process)

For FLAC analyses, seismic input must be applied at the base of the model. Therefore, the acceleration time history at the base of the model must be determined from the acceleration time history at bedrock level. The acceleration time history at the base of the FLAC model is determined using the deconvolution process using the equivalent-linear 1D wave propagation code SHAKE91.

The upward-propagating wave motion (1/2 the outcrop motion) is extracted from SHAKE at the top of the layer at a depth of 12 meters, which is the height of the soil foundation being modeled in the FLAC model. The outcrop motion needed to be baseline corrected to avoid having uncorrected residual displacement at the end of the dynamic analysis (Figure 3). Figure 4 illustrates the acceleration propagation through soil layers by comparing the applied selected motion at bedrock and outcrop motion at the base of the FLAC model after being baseline corrected. This acceleration-time history was integrated to obtain a velocity, which was then converted to stress history. The acceleration-stress history is utilized for the dynamic analysis of the FLAC model.

3.3.3.   Numerical Dynamic analysis

After static analysis of the FLAC model is completed, the static boundary conditions of the model are changed to dynamic boundary conditions. The free-field boundary condition is specified to the lateral outer boundaries of the model. The

boundaries must be vertical, straight, and positioned at the lower-left and lower-right corners of the model based on FLAC 2D Dynamic Analysis manual. Quiet boundaries were applied in both x and y direction at the base of the model.

When applying velocity or acceleration input to the model boundaries, quiet boundaries would nullify these input accelerations. Therefore, the acceleration time history converted to a velocity first. Secondly, the velocity wave converted to a shear-stress history by multiplying by the stress factor (applied shear stress). The applied shear stress is determined from the following equation:

$$\sigma_s = 2 \, \rho \, C_s \, V_s \tag{2}$$

Where σ_s is applied shear stress, ρ is mass density of the materials located at the base of the model, C_s is speed of shear-wave propagation of the base soil layer and V_s is input shear particle velocity. Then, the shear-stress history can be assigned to the quiet boundary in the FLAC model which is the base of the model.

It should be taken into account that by having the output motion as outcrop motion for the base of the FLAC model from SHAKE, there was no need to use multiplication of two in the previous equation. Because the acceleration values of outcrop had both upward and downward motion and needed to be divided by two. So, the stress factor that was used is:

$$\sigma_s = (1762 \, kg/m^3)(242 \, m/s)V_s = 426404 \, V_s$$

4. Results and discussion
4.1. Vertical Stresses

A primary objective of determining stresses from anticipated earthquakes is to select the proper type of EPS that can support the anticipated increase in stress due to

dynamic stresses. One alternative of evaluating the stresses provided by the FLAC model within the EPS embankment is to subdivide the EPS embankment into zones. Therefore, the 33 m wide by 12 m high EPS embankment is initially divided into 52 zones with each zone having a width of 8.25 m and thickness of 1 m as shown in Figure 5.

Figure 6 shows the locations of six vertical stress points provided by the FLAC model. Stress points 1, 2, and 4, 5 provide a total of four stress points at the corners of the zone and Stress points 3 and 6 provide two stress points at the top and bottom, respectively, of the center of the zone.

Table 5 provides a summary of vertical stress values obtained at the center and bottom, i.e., Point 6, of each zone. The depth values in Column 1 of Table 5 are depths from the top of the EPS embankment to the bottom of the embankment. Three vertical stress values representing the static stress prior to the earthquake, the dynamic and static stress towards the end of the earthquake, and the maximum dynamic and static stress obtained during the earthquake are provided for each zone. Negative stresses indicate downward stresses. The maximum static and dynamic stresses obtained during the earthquake at each depth typically occur at different time intervals during the earthquake. The earthquake dynamic analysis does not include live load stresses imposed by vehicles at the top of the pavement system. Therefore, the stresses indicated in Table 5 do not include live load vehicle stresses.

The 2020 edition of the AASHTO LRFD Bridge Design specifications (AASHTO 202) indicates that past editions of the specifications used a load factor of 0 to live load but that the possibility of partial live load with earthquakes be considered.

The AASHTO (2020) specifications indicate that the load factor for live load shall be determined on a project-specific basis. As noted in Figure 5 and Table 5, the critical portions of the embankment where the sum of static and dynamic stresses are the greatest are located at the outer and bottom corners of the embankment at approximately 9 m in depth. Live loads are anticipated to be minimum at these depths. Therefore, not including live load vehicle stress in the FLAC analysis for the EPS embankment of this study is reasonable.

A key objective in design of EPS embankments is to select an EPS type that has an elastic limit stress that is greater than the anticipated stresses that will be imposed on the EPS blocks. The elastic limit stress is defined as the compressive resistance at 1 percent strain. Therefore, to better evaluate the stress ranges anticipated within a given row of EPS blocks within each embankment zone, the average of the maximum static and dynamic stress obtained during the earthquake at each of the six points shown in Figure 6 was determined for each zone and these average maximum static and dynamic stresses are summarized in Table 6.

The maximum static and dynamic stress values used in determining the overall maximum average is based on the maximum vertical stress obtained at each point within a zone as shown in Figure 6 during the earthquake. The maximum stress that occurs at each point within a zone occurs at different times during the earthquake. Therefore, the maximum stress values shown in Table 6 for each zone represent the average of the maximum stresses obtained at each of the six points within the zone as shown in Figure 6 at various times during the earthquake.

Table 6 also provides the EPS types proposed for the embankment as well as the

elastic limit stress values provided in ASTM D6817 (ASTM International 2017) for the

given EPS type. As indicated in Table 6, the average of the maximum static and

dynamic stress obtained during the earthquake at each of the six points shown in Figure

6 that are highlighted in yellow exceeds the elastic limit stress of the EPS type near the

outer and bottom corners of the embankment in eight zones. Therefore, to better

determine the extent of where the dynamic and static stresses exceed the elastic limit

stress of the EPS, the stresses were reevaluated by further subdividing these eight zones

in half vertically to create 16 zones as shown in Figure 7. The additional zones are

designated as Columns 1 through 4 as shown in Figure 7.

Table 7 provides a summary of the maximum static and dynamic stresses

obtained in each of the 16 zones shown in Figure 7. The maximum stresses shown in

Table 7 represent the maximum stress obtained during the earthquake within each zone

and not the average of the maximum stresses obtained during the earthquake at each of

the six points shown in Figure 6 because no portion of the EPS block should exceed the

elastic limit stress.

Table 7 also provides the EPS type and elastic limit stress for each EPS type

proposed for the embankment. As indicated in Table 7, the estimated sum of dynamic

and static stresses highlighted in yellow from the FLAC dynamic analysis exceeds the

elastic limit stress of the EPS type at Columns 1 and 4, which is the extreme outer

corners of the embankment.

Table 8 provides revised EPS types with elastic limit stresses that exceed the

estimated maximum dynamic and static stresses along Columns 1 and 4 shown in

Figure 7. As shown in Table 8, substituting EPS 29 and EPS 39 for the proposed EPS 22 within Column 1 and 4 areas of the embankment would provide elastic limit stresses that exceed the estimated static and dynamic stresses. The selection of the revised EPS types does not include the use of a factor of safety of 1.2 that the NCHRP 529 Report (Stark et al. 2004) suggests being applied to the estimated anticipated maximum stresses, i.e., required elastic limit stress = 1.2 × estimated anticipated maximum stress, nor does it include live loads from traffic. AASHTO (2020) suggests a load factor of 1 for Extreme Event I limit state. Therefore, not incorporating a factor of safety for evaluation of temporary seismic dynamic stresses is reasonable. As previously indicated, not including live loads from traffic is also reasonable for the EPS embankment of this study.

The results of the FLAC dynamic analyses are based on the recommendations of the NCHRP 529 report (Stark et al. 2004a) that overall estimated stresses that will be imposed on the EPS blocks do not exceed the elastic limit stress of the EPS type. As previously noted, the elastic limit stress is defined as the compressive resistance at 1 percent strain. However, a more recent study by Bartlett and Neupane (2017), suggests that for the design of EPS bridge support systems for temporary seismic loads, EPS with a compressive resistance measured at 2% axial strain, can be used for the selection of EPS type.

The current ASTM D6817 (ASTM D6817) provides minimum compressive resistance values at 1%, 5%, and 10% strains but not at 2% strain. Bartlett and Neupane (2017) suggest that the compressive resistance at 2% axial strain is approximately equivalent to 85 percent of the compressive resistance at 10 percent provided the EPS blocks have stress-strain behavior similar to EPS 25. EPS 25 is not an EPS type

provided by ASTM D6817. Additionally, EPS 22 is being proposed for the Poplar Avenue bridge replacement embankment project. Thus, one challenge of the 2% axial strain analysis is to determine if the Bartlett and Neupane suggestion that the compressive resistance at 2 % axial strain is approximately equivalent to 85 percent of the compressive resistance at 10 percent is applicable to EPS 22. This determination was made by calculating the ratio of the stress at 2% strain to 10% strain of various EPS types from the results of monotonic uniaxial tests conducted by Bartlett and Neupane (2017). Table 9 provides a summary of the ratios.

As noted in Table 9, the ratio of the stress at 2% strain to 10% strain, which is expressed in percent, increases with increase in EPS density. EPS 22 that has a minimum density of 21.6 kg/m^3 per ASTM D6817 was not tested by Bartlett and Neupane. Conservatively, the 76% ratio of EPS 19 with a density of 20.2 kg/m^3 from Table 9 is also used for EPS 22 in the dynamic analysis herein. Thus, the compressive resistance at 2 % axial strain for EPS 22 is estimated to be approximately 76 percent of the compressive resistance at 10 percent, which is 135 kPa (19.6 psi) per ASTM D6817. Thus, the estimated compressive resistance at 2 % axial strain for EPS 22 is 103 kPa (15 psi). It should be noted that a more comprehensive test program than the Bartlett and Neupane monotonic uniaxial test results of Table 9 is suggested to obtain a more reliable correlation between the compressive resistance at 2 % axial strain and 10% strain for all EPS types including EPS 22.

Table 10 is similar to Table 7except that Table 10 provides the estimated compressive resistance at 2% strain for EPS 22 of 103 kPa (15 psi) instead of the elastic limit stress included in Table 7. As noted in Table 10, a comparison of the maximum static and dynamic stresses in each of the 16 zones shown in Figure 7 indicates that the

estimated sum of dynamic and static stresses does not exceed the compressive resistance at 2% strain of EPS 22. Therefore, EPS 22 can be considered an acceptable EPS type under static and dynamic stresses based on the 2% strain criterion. The 2% criterion provides an economical advantage compared to the 1% criterion because the cost of EPS 22 is less than the cost of EPS 29 and EPS 39. EPS 22 has a lower density than EPS 29 and EPS 39 and the cost of EPS blocks increases with density.

4.2. Sliding evaluation

The purpose of a sliding evaluation analysis is to evaluate potential horizontal displacements that may occur between rows of EPS blocks during a seismic event. The sliding potential of EPS layers is evaluated by using the strain function in FLAC. Table 11 provides the maximum relative horizontal displacement that occurred during an earthquake, cumulative maximum horizontal displacement, and anticipated cumulative displacement after an earthquake at each EPS interface at the middle (center) and left side of the embankment. The displacement at the right side of the embankment is assumed to be the same as the left side so only left side displacements are provided. Figure 8 illustrates the horizontal relative displacement histories for all of the EPS layers as well as the top of the pavement.

The maximum relative X-displacement indicated in Table 11 is the maximum displacement that was obtained during the earthquake between the bottom of the upper block and bottom of the lower block at each EPS block interface. These maximum displacement values at various heights of the EPS embankment occur at different times during the earthquake. Negative displacements are displacements that occur to the left and positive displacements are displacements that occur to the right.

The cumulative X-displacement values indicated in Table 11 represent the overall sum of maximum relative displacements from the EPS Layer 1 to EPS Layer 2 interface to a given upper EPS interface level. For example, the cumulative displacement at the left side at the EPS Layer 3 to EPS Layer 4 interface is 1.96 cm + (-1.51 cm) + (-1.36 cm) = -0.91 cm. Therefore, since the cumulative displacement at a given height within the EPS embankment is the sum of maximum displacements at each interface below the given height, the cumulative X-displacement values can be considered the estimated upper limits of X-displacement that may occur during the earthquake.

The overall cumulative displacement at the top of the EPS values indicated at the bottom row of the cumulative X-displacement column of Table 11 represents the overall sum of maximum relative displacements from the extreme bottom of the EPS embankment to the extreme top of the EPS embankment and is the anticipated relative displacement at the top of the EPS embankment. Estimated overall cumulative displacements at the top of the EPS of 11.00 cm and 12.13 cm for the left boundary and the middle points, respectively. Therefore, the cumulative X-displacement values obtained from the FLAC analysis suggest potential maximum horizontal displacements of up to 12 cm during an earthquake similar to the earthquake used in the FLAC analysis.

The anticipated cumulative displacement after earthquake values indicated in Table 11 is the cumulative displacement obtained at a given interface that is determined by adding all the back-and-forth horizontal displacements that occur in the FLAC model during the full earthquake time history. Thus, the anticipated cumulative displacement at the end of the earthquake at a given interface can be considered the estimated lower

limit of X-displacement that may occur at the end of the earthquake. The anticipated cumulative displacement values obtained at the end of the earthquake suggest anticipated cumulative displacements of up to 1 cm.

In summary, the cumulative X-displacement values obtained from the FLAC analysis suggest potential maximum horizontal displacements of up to 12 cm during an earthquake like the selected earthquake used in the FLAC analysis. The anticipated cumulative displacement values obtained at the end of the earthquake suggest anticipated cumulative displacement of up to 1 cm.

4.3. Conclusions

This study provides a methodology for analyzing the load-bearing capacity and horizontal sliding failure mechanisms that are required to complete a seismic internal stability analysis of EPS-block geofoam embankments. The objective of the seismic analysis procedure is to determine stresses from anticipated earthquakes to select the proiper type of EPS that can support the anticipated increase in stress due to dynamic stresses and to evaluate potential horizontal displacements that may occur between rows of EPS blocks during a seismic event. The seismic analysis procedure considers the additional stresses due to rocking of the embankment and the impact of lateral sway and damping on horizontal sliding between rows of EPS blocks. The procedure considers both the 1% and 2% strain criteria for selecting the proper EPS block types to support both dynamic and static stresses.

The methodology for performing numerical seismic analysis of an EPS-block embankment consists of the following steps: (1) developing the FLAC numerical model, (2) determining acceleration time histories, and (3) performing the numerical

dynamic analysis. The procedure for Step 2, determining time histories, consist of the following sub steps: (1) obtaining the target response spectrum, (2) selecting appropriate ground motions, (3) obtaining bedrock surface level and shear wave velocity, (4) determining acceleration time histories at the base of the FLAC model (the deconvolution process).

The seismic analysis procedure is demonstrated by analysis of one of the EPS-block geofoam embankments that TDOT is proposing as partial replacement of an existing bridge in Memphis, Tennessee in the USA. The FLAC dynamic analysis results indicate that the static and dynamic stresses can exceed the elastic limit stress of the proposed geofoam type EPS 22 along the extreme outer corners of the embankment. Substituting EPS 29 and EPS 39 for the proposed EPS 22 within Column 1 and 4 areas of the embankment as depicted in Figure 3 would provide elastic limit stresses that exceed the estimated static and dynamic stresses. However, the results of a re-analysis of dynamic stresses of the embankment based on the 2% axial strain criterion indicate that EPS 22 can be considered an acceptable EPS type. Therefore, the 2% criterion provides an economical advantage compared to the 1% criterion because the cost of EPS 22 is less than the cost of EPS 29 and EPS 39.

This study has presented a method to incorporate the 2% criterion because currently there is limited EPS test data that provides compressive resistance values at 2% strain. It is recommended that a more comprehensive test program be performed to obtain a more reliable correlation between the compressive resistance at 2 % axial strain for all EPS types.

Although the 2% axial strain criterion is based on limited test data, if static and temporary dynamic stresses do exceed the cyclic elastic limit of the EPS, the potential consequence can be that long-term creep strains after the earthquake event may be greater than anticipated resulting in overall settlement of the embankment that can be greater than anticipated. However, the additional deformation and settlement of the embankment would typically not result in catastrophic collapse, which is in general agreement with the 'no-collapse' philosophy for seismic design that has been adopted by many state and federal agencies (Marsh et al. 2014).

The results of the Memphis EPS embankment also indicated that not including live load vehicle stress in the FLAC analysis and not incorporating a factor of safety for evaluation of seismic dynamic stresses appear to be reasonable seismic analysis approaches based on the AASHTO (2020) specifications.

The interlayer sliding potential at each horizontal EPS interface resulted in a maximum overall cumulative horizontal displacement of 1.11 cm of one layer and 12.13 cm for the entire embankment comparing the bottom and top of the embankment that occurred during an earthquake. The maximum anticipated relative displacement value was about 0.97 cm for one of the layers and the values obtained at the end of the earthquake suggest anticipated cumulative displacements of up to 1 cm. The cumulative horizontal displacement values obtained from the FLAC analysis suggest potential maximum horizontal displacements of up to 12 cm during an earthquake like the earthquake used in the FLAC analysis.

Acknowledgements

This work performed for this study was supported by the Tennessee Department of Transportation (TDOT) and by the Department of Civil Engineering at the University of Memphis.

References

AASHTO *LRFD bridge design specifications*. 2020. Ninth edition. American Association of State Highway and Transportation Officials, Washington DC. USA. ISBN-10: 1560517387 ISBN-13: 978-1560517382.

Arellano, D., and T. D. Stark. 2009. "Load bearing analysis of EPS-block geofoam embankments." *Bearing Capacity of Roads, Railways and Airfields - Proceedings of the 8th International Conference on the Bearing Capacity of Roads, Railways and Airfields*, E. Tutumluer & I.L. Al-Qadi (eds), CRC Press/Balkema, The Netherlands, Vol. 2, pp. 981-990.

Arellano, D., T. D. Stark, J. S. Horvath, D. Leshchinsky, M. H. Kafash, and C. Wang. 2011. "Overview of NCHRP Design Guideline for EPS-Block Geofoam in Slope Stabilization and Repair." *Proceedings of the 4th International Conference on the use of Geofoam Blocks in Construction Applications*. Norway.

Arellano, D., T. D. Stark, J. S. Horvath, D. Leshchinsky, 2013. National Cooperative Highway Research Program, Transportation Research Board, and National Academies of Sciences, Engineering, and Medicine. *Guidelines for Geofoam Applications in Slope Stability Projects*. 22630. Washington, D.C.: Transportation Research Board.

Arellano, D., J. B. Tatum, T. D. Stark, J. S. Horvath, and D. Leshchinsky. 2010. "Framework for Design Guideline for Expanded Polystyrene Block Geofoam in Slope Stabilization and Repair." *Transportation Research Record*, 2170 (1): 100–108. SAGE Publications Inc. https://doi.org/10.3141/2170-12.

ASTM Standard D6817, 2017. Specification for Rigid Cellular Polystyrene Geofoam. ASTM International, West Conshohocken, PA. DOI: 10.1520/D6817_D6817M-13A.

Amini, Z., 2014. "Dynamic characteristics and seismic stability of expanded polystyrene geofoam embankments" (Doctoral dissertation). The University of Utah, Salt Lake City, UT.

Bartlett, S. F., and R. Neupane. 2017. "Seismic Evaluation of Expanded Polystyrene (EPS) Geofoam Bridge Support System for Overpass Structures." *North Dakota State University - Upper Great Plains Transportation Institute*, Fargo: Mountain-Plains Consortium Report MPC 17-328.

Bartlett, S., C. Person, and E. Lawton. 2008. "Evaluating the Seismic Stability and Performance of Freestanding Geofoam Embankment". *6th National Seismic Conference on Bridges and Highways*. Charleston, South Carolina, USA. DOI: 10.13140/2.1.2399.7449

Horvath, J. S. 1995. "Geofoam Geosynthetic". *Horvath Engineering, P.C.*, Scarsdale, NY, USA. July 1995, 229 pp.

Horvath, J. S. 2004. "A Technical Note re Calculating the Fundamental Period of an EPS-Block-Geofoam Embankment". *Geomaterials Research Project*. DOI: 10.13140/RG.2.2.23509.27369

Horvath, J. S. 2011. "Discussion of 'Numerical Modeling of Geofoam Embankments' by M. P. Newman, S. F. Bartlett, and E. C. Lawton." *Journal of Geotechnical and Geoenvironmental Engineering*, 137 (8): 814–817. American Society of Civil Engineers. https://doi.org/10.1061/(ASCE)GT.1943-5606.0000416.

Horvath, J. S. 2012. "Lateral Pressure Reduction on Earth-Retaining Structures Using Geofoams: Correcting Some Misunderstandings." 862–869. American Society of Civil Engineers. https://doi.org/10.1061/41128(384)86.

Horvath, J. S., T. Stark, D. Arellano, and D. Leshchinsky. 2004a. "NCHRP Report 529: Guideline and Recommended Standard for Geofoam Applications in Highway Embankments", *Transportation Research Board*, Washington, D.C., 71 pp.

Horvath, J. S., T. Stark, D. Arellano, and D. Leshchinsky. 2004b. "NCHRP Web Document 65 (Project 24-11): Geofoam Applications in the Design and Construction of Highway Embankments". *Transportation Research Board*, Washington, D.C., 792 pp.

Hu, J. S., J. Ren, and D. Wu. 2019. "Dynamic Mechanical Properties of EPS Concrete Under Impact Loading." *J. Shanghai Jiaotong Univ. (Sci.)*, 24 (1): 94–100. https://doi.org/10.1007/s12204-019-2042-1.

Itasca Consulting Group, Inc. 2019. FLAC — Fast Lagrangian Analysis of Continua, Ver. 8.1. Minneapolis: Itasca. https://www.itascacg.com/software/FLAC.

Marsh, M. L., I. G. Buckle, and E. Kavazanjian Jr. 2014. "LRFD Seismic Analysis and Design of Bridges Reference Manual: NHI Course No. 130093 and 130093A."

PEER Ground Motion Database - Pacific Earthquake Engineering Research Center. 2013. https://ngawest2.berkeley.edu/.

Riad, H., and J. Horvath. 2004. "Analysis and Design of EPS-Geofoam Embankments for Seismic Loading". *Geotechnical Engineering for Transportation Projects* (GSP 126), ASCE, Reston, VA, 2028–2037.

Schaefer, V. R., Berg, R. R., Collin, J. G., Christopher, B. R., DiMaggio, J. A., Filz, G. M., Bruce, D. A., and D. Ayala. 2016. "Geotechnical Engineering Circular No. 13 Ground Modification Methods - Reference Manual: volume I, Report No. FHWA-NHI-16-027", *National Highway Institute, U.S. Department of Transportation, Federal Highway Administration*, Washington, DC 20590.

Transportation Research Board and National Academies of Sciences, Engineering, and Medicine. 2004. *Guideline and Recommended Standard for Geofoam Applications in Highway Embankments*. 13759. Washington, D.C.: Transportation Research Board.

United States Geological Survey (USGS), 2019, USGS Unified Hazard Tool (Deaggregation) website. https://earthquake.usgs.gov/earthquakes/search/.

Appendix A: The numerical modeling validation

The duplication analysis consists of modeling a 10 m width by 5 m height EPS embankment performed as one of the initial steps toward numerical model used in this study based on Bartlett and Lawton (2008) research and their numerical model and EPS seismic analysis results. As shown by Figure A1, the model consists of a rectangular geofoam embankment resting on a soil foundation with sliding allowed within the geofoam, at the geofoam/foundation and pavement system/geofoam interfaces under a horizontal sinusoidal input motion. Figures A2 and A3 and Table A1 shows that the duplication analysis agrees with the results obtained by Bartlett and Lawton with precisely the same seismic analysis results. All the values for horizontal displacement and accelerations were completely matched and compared with the authors' numerical model to validate the EPS modeling with FLAC and under seismic loads.

Dr. Bartlett's study   Duplication analysis by Marzieh
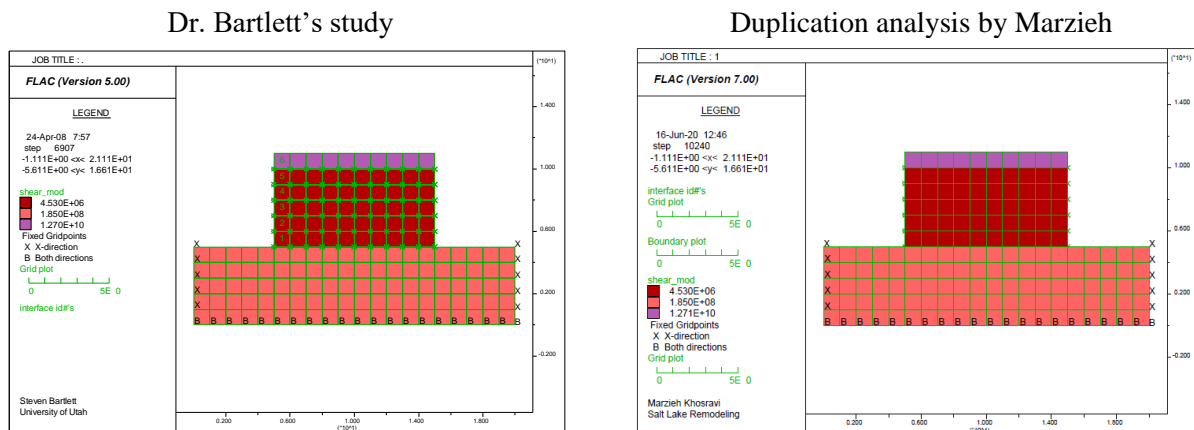
Figure A1. Boundary conditions and shear modulus of the properties.
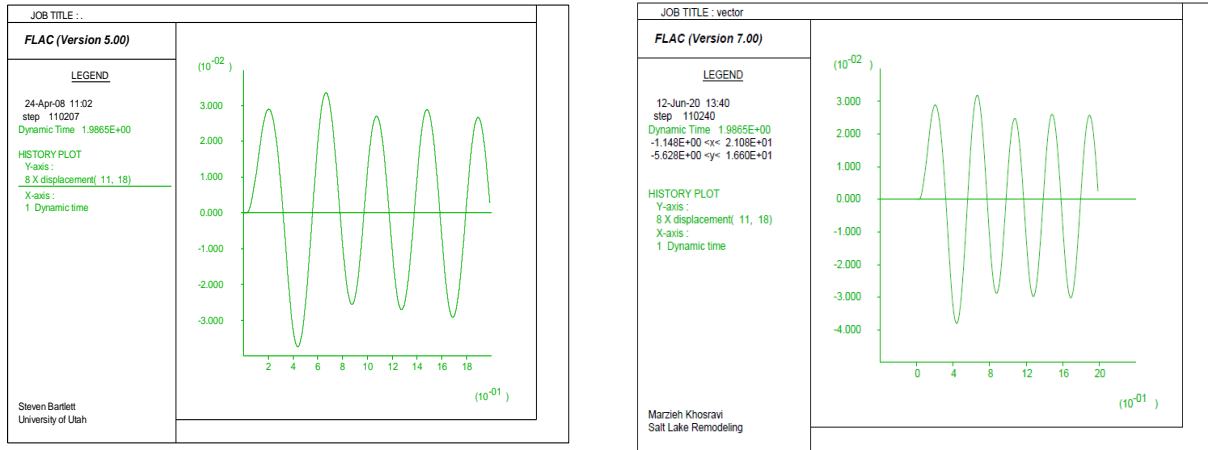
Figure A2. Horizontal displacement at surface of the pavement near the center.
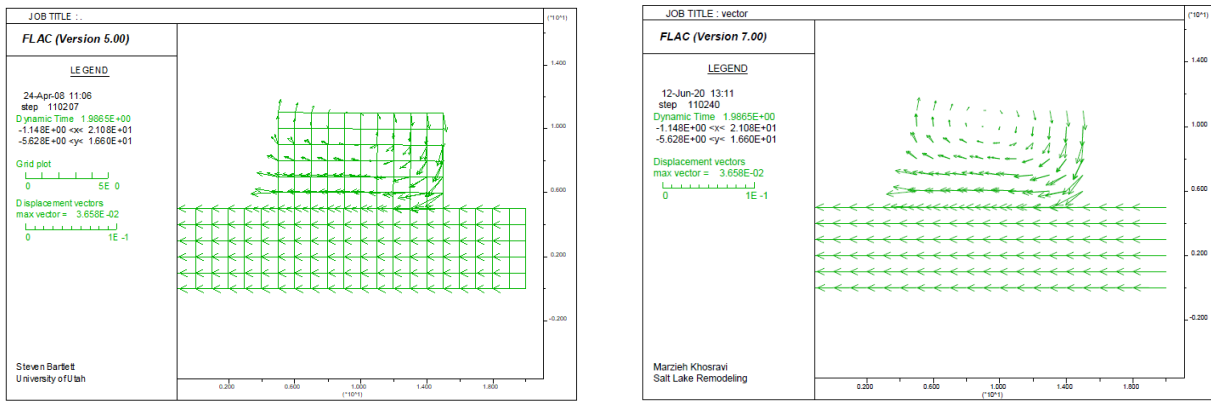
Figure A3. Displacement vectors at dynamic time of 1.98 sec.

Table A1. Comparison of dynamic analysis.

	Bartlett and Lawton (2008)	Khosravi (2020)
Dynamic Time	1.9865	1.9865
Number of steps for dynamic analysis	110207	110240
Horizontal displacement at base	4.2 (cm)	4.24 (cm)
Horizontal displacement at top	3.2 (cm)	3.188 (cm)
Horizontal acceleration at base	9.9 (m/s^2)	9.95 (m/s^2)
Horizontal acceleration at top	6.6 (m/s^2)	6.75 (m/s^2)
Max displacement vector at dynamic time = 4 sec	3.658 (cm)	3.658 (cm)

Manuscript's Figures
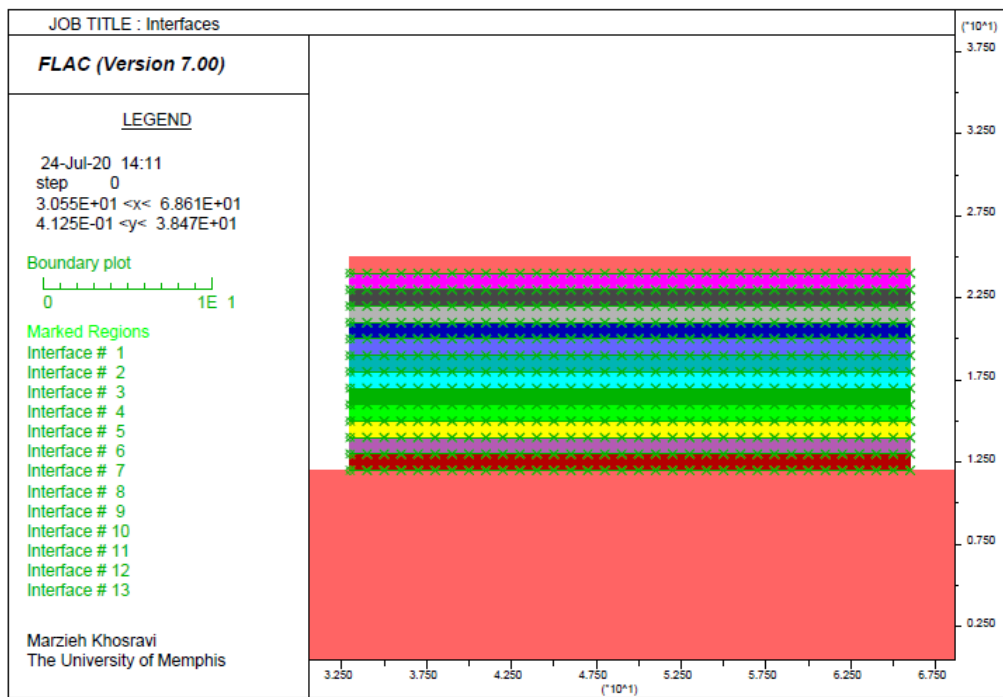
Figure 1. FLAC model showing soil foundation and horizontal interfaces modeled for the EPS embankment
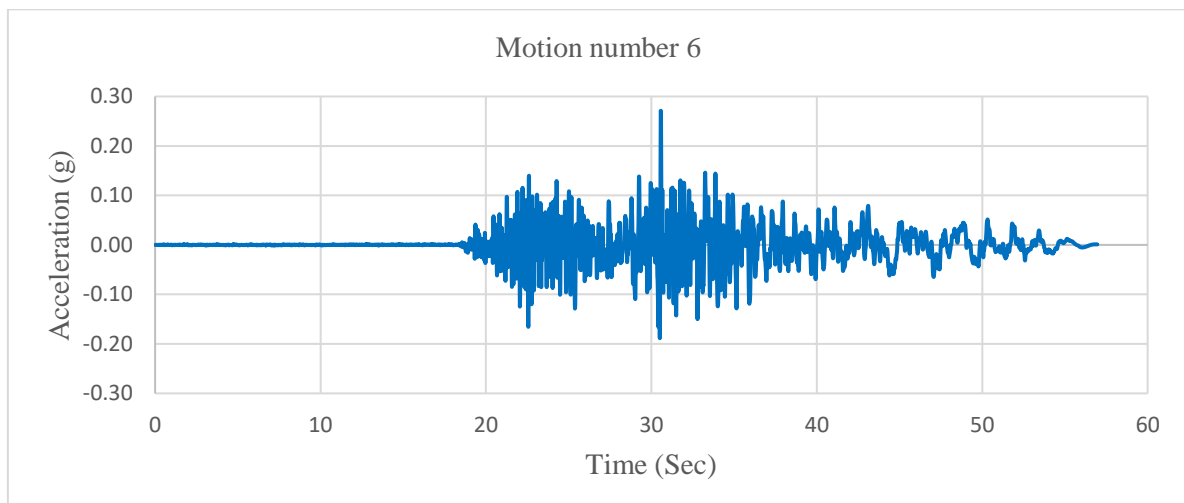
Figure 2. Record Sequence Number (RSN) 2924 Chi-Chi-Taiwan-04 (1999) time history of horizontal acceleration.
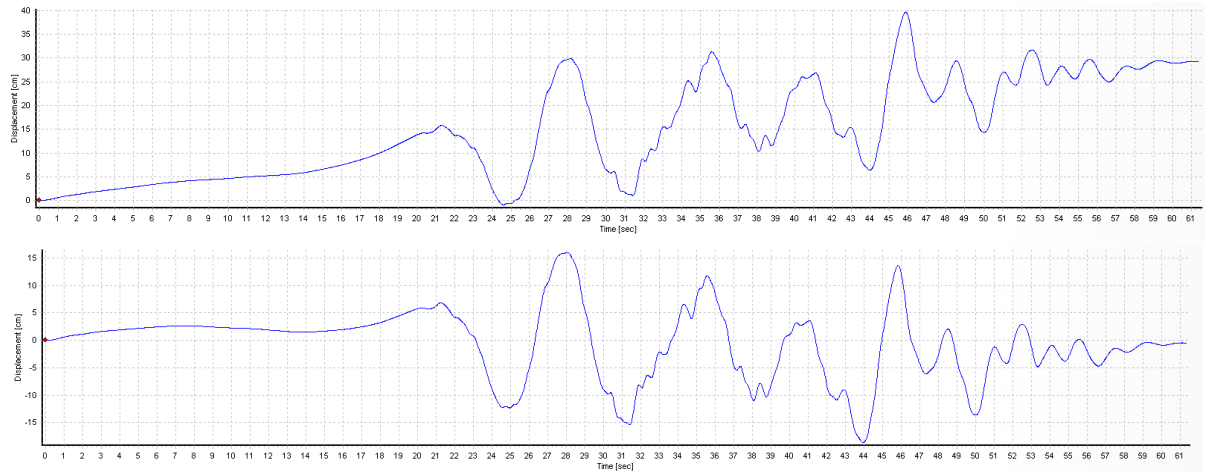
Figure 3. Displacement (cm) versus time (sec): a) uncorrected baseline, b) corrected baseline.
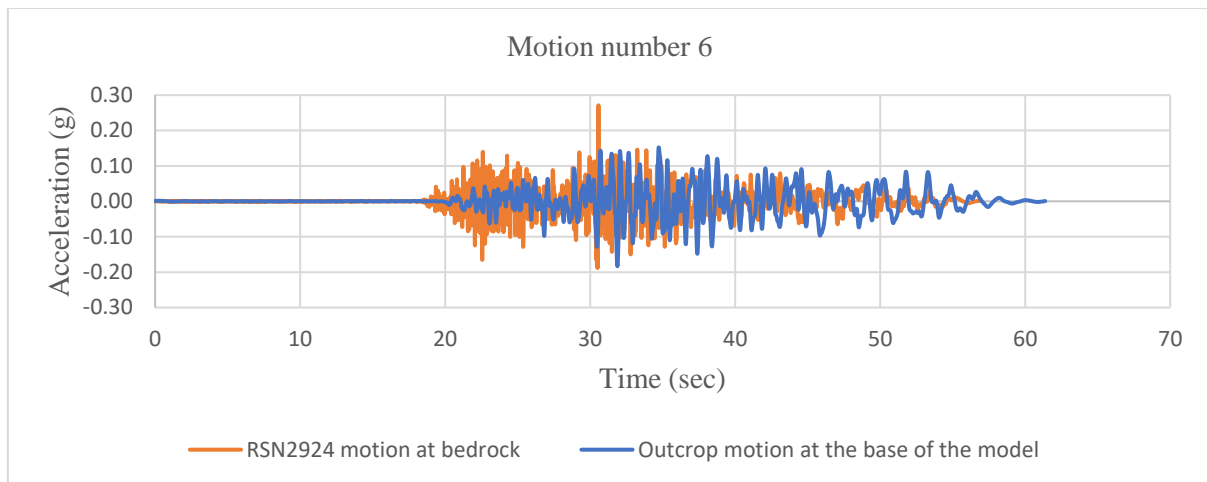
Figure 4. Acceleration propagation through soil layers for the selected motion.
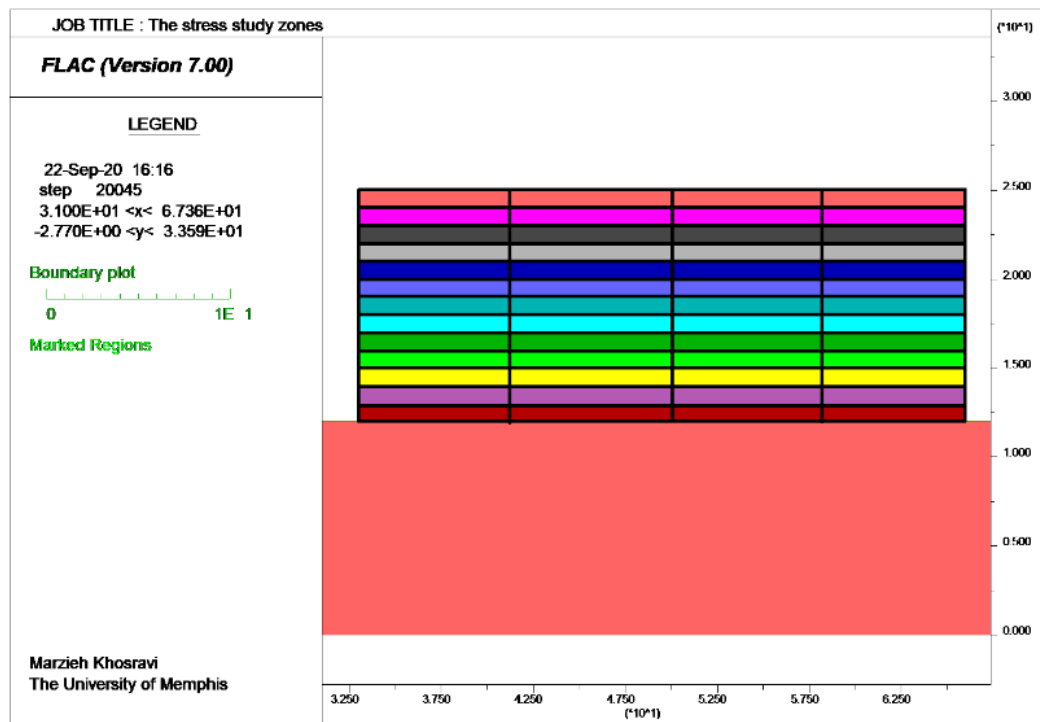
Figure 5. Model showing 52 EPS block zones utilized to determine vertical stresses.
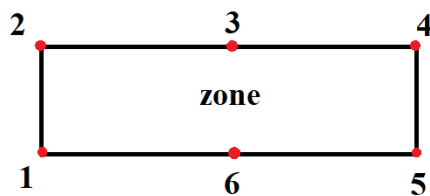
Figure 6. Location of vertical stress points for each zone.
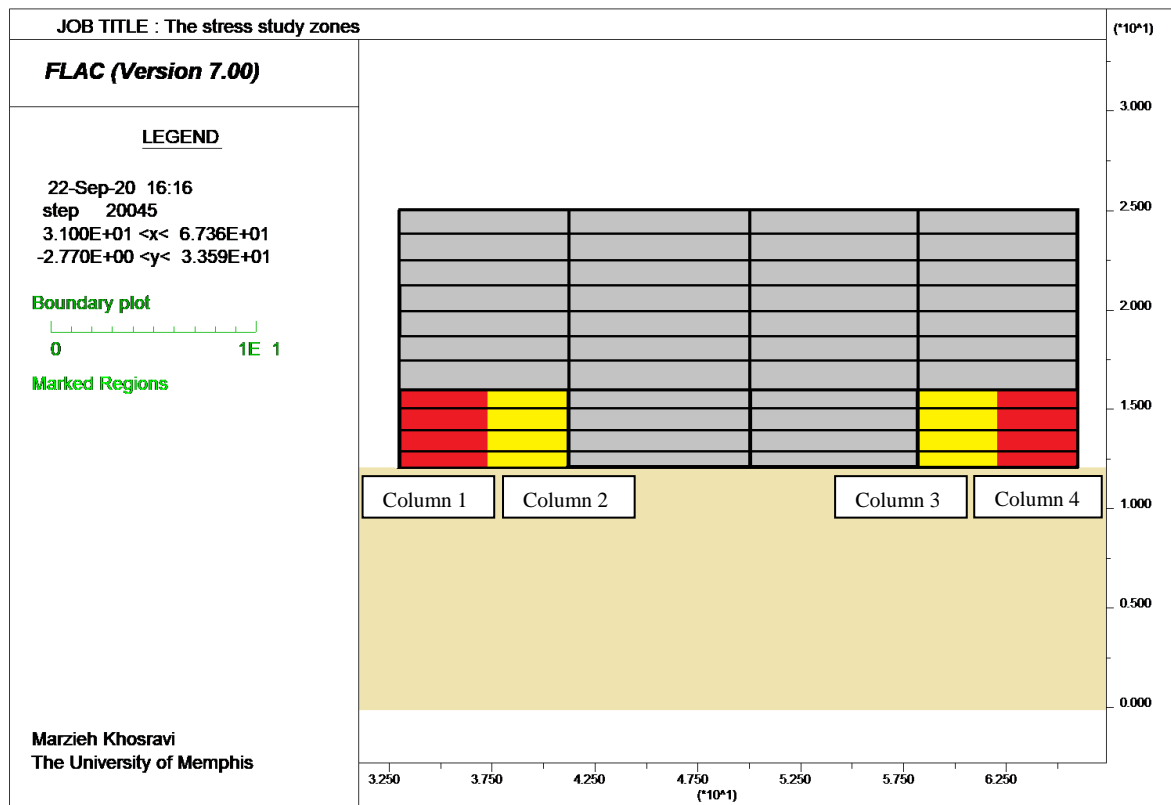
Figure 7. Additional zones used for further vertical stresses analyze.
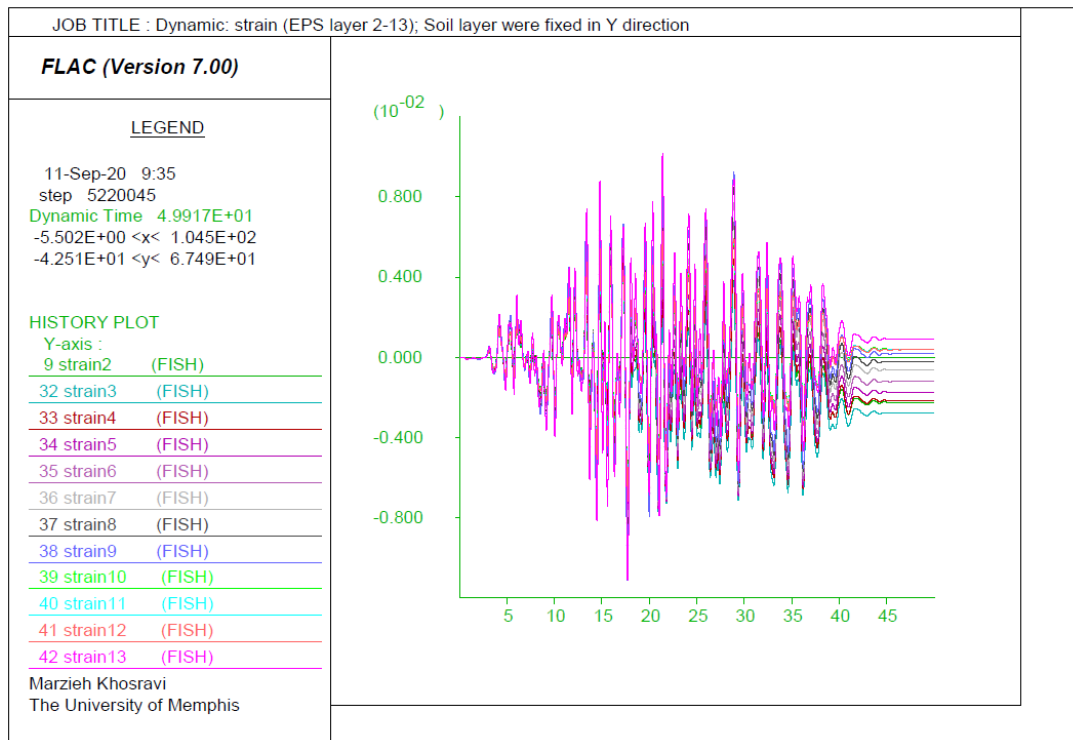
Figure 8. The horizontal relative displacement histories for all of the EPS layers and top pavement

Manuscript's Tables

Table 1. Model dimensions.

	Soil Foundation (m)	EPS (m)	Pavement System* (m)
Width	99	33	33
Height	12	12	1

*Pavement System is a section at the top of the EPS embankment representing the combined load distribution slab and pavement section with the average height of 1 meter.

Table 2. Model properties.

Material	type	Location[a]	density kg/m^3	Elastic Modulus (E) MPa[b]	Poisson ratio	Bulk modulus (K) MPa	Shear modulus (G) MPa
EPS	EPS 22	8 layers	21.6	5.00	0.12	2.19	2.23
	EPS 39	Top 4 layers	38.4	10.30	0.23	6.35	4.19
Pavement System			2300	30.00	0.18	15625	12718
Soil Layers	Clayey silt, ML	0-7 (m)	1506	4.79	0.35	1.77	5.32
	Sandy Clay, CL	7-9 (m)	1570	5.99	0.3	2.3	4.99
	Clayey Sand, SC	9-11 (m)	1698	34.47	0.4	12.31	57.46
	Sand, SP	11-12 (m)	1762	43.09	0.4	15.39	71.82

[a] Zero elevation assumed to be the ground surface.
[a] Compressive resistance at 1% strain from ASTM and divide by 1%, based on ASTM D6817-17 for EPS.

Table 3. Interfaces properties used for sliding evaluation in the FLAC model.

Contact surface	Interface number	Type	Normal and Shear Stiffness ($k_n = k_s$) (MPa)	Friction angle (degree)
Soil foundation/EPS 22	1	Glued	258	31
EPS22/EPS22	2 to 8	Not glued	258	38
EPS 22/EPS39	9	Not glued	258	38
EPS39/EPS39	10 to 12	Not glued	597	38
EPS 39/ Pavement System	13	Glued	597	38

Table 4. Horizontal strong motion records selected for evaluations.

Motion Number	Mean Squared Error	Scale Factor	Earthquake Name	Magnitude (g)	Rrup (km)
1	0.03	3.71	1999 Chi-Chi_ Taiwan-04	6.2	39.3
2	0.04	2.44	1989 Loma Prieta	6.93	55.1
3	0.07	6.04	1999 Chi-Chi_ Taiwan-04	6.2	50.8
4	0.09	2.79	1999 Duzce_ Turkey	7.14	25.9
5	0.1	3.59	2008 Iwate_ Japan	6.9	57.2
6	0.12	6.74	1999 Chi-Chi_ Taiwan-04	6.2	60.8
7	0.13	4.38	1999 Chi-Chi_ Taiwan-05	6.2	45

Table 5. Comparison of vertical stresses before the earthquake (static loads), near end of earthquake, and maximum during earthquake for the middle and bottom point (Point 6) for each zone

Depth (m)	Vertical stress values: Before/end/maximum during an earthquake for Point 6 of each zone, kPa			
0-1	-10.96/-11.4/-16.27	-10.97/-11.27/-14.05	-10.98/-11.74/-14.04	-10.97/-10.14/-17.26
1-2	-22.36/-23.34/-33.83	-22.21/-22.66/-28.21	-22.21/-23.68/-28.28	-22.38/-20.76/-38.6
2-3	-23.15/-24.11/-35.44	-22.68/-23.00/-28.68	-22.68/-24.07/-28.93	-23.17/-28.15/-37.35
3-4	-23.84/-24.68/-36.6	-23.14/-23.47/-29.16	-23.14/-24.46/-29.52	-23.85/-23.46/-39.18
4-5	-24.37/-24.98/-37.94	-23.58/-24.08/-29.6	-23.58/-24.47/-29.93	-24.37/-25.17/-40.58
5-6	-24.67/-24.42/-39.14	-23.93/-24.36/-29.74	-23.93/-24.35/-30.16	-24.67/-26.38/-41.46
6-7	-24.80/-25.09/-40.58	-24.17/-23.72/-29.75	-24.16/-24.71/-30.15	-24.80/-27.21/-42.1
7-8	-24.86/-25.40/-41.91	-24.41/-23.89/-30.02	-24.41/-24.90/-30.43	-24.85/-28.10/-42.7
8-9	-24.85/-25.40/-43.22	-24.64/-25.95/-30.27	-24.64/-23.55/-30.11	-24.85/-25.74/-42.55
9-10	-24.76/-27.15/-44.06	-24.86/-25.99/-31.00	-24.86/-22.48/-30.26	-24.75/-26.90/-44.9
10-11	-24.58/-25.62/-44.20	-25.07/-25.55/-30.98	-25.07/-22.75/-30.41	-24.60/-23.50/-43.7
11-12	-24.44/-26.00/-42.85	-25.29/-25.57/-30.99	-25.29/-23.34/-30.64	-24.44/-29.90/-43.46
12-13	-24.30/-23.50/-41.1	-25.50/-26.35/-31.4	-25.51/-24.02/-30.78	-24.30/-20.00/-42.1

Table 6. Comparison between vertical stress before an earthquake (static loads) and average maximum statis and dynamic stress of all six points shown in Figure 6 obtained in each zone during the earthquake.

Depth (m)	EPS Type (Elastic limit stress, kPa)	Vertical stress values: Before earthquake (static loads) / average maximum static and dynamic stress of all six points shown in Figure 6, kPa			
0-1	EPS30	-10.96/-23.61	-10.97/-16.13	-10.98/-15.78	-10.97/-23.74
1-2	(103)	-22.36/-43.24	-22.21/-33.14	-22.21/-32.37	-22.38/-43.29
2-3		-23.15/-43.24	-22.68/-34.32	-22.68/-33.35	-23.17/-43.29
3-4		-23.84/-38.06	-23.14/-35.24	-23.14/-34.33	-23.85/-39.18
4-5	EPS 22	-24.37/-37.94	-23.58/-36.09	-23.58/-35.24	-24.37/-40.58
5-6	(50)	-24.67/-39.14	-23.93/-36.44	-23.93/-35.96	-24.67/-41.46
6-7		-24.80/-40.58	-24.17/-36.5	-24.16/-36.59	-24.80/-42.1
7-8		-24.86/-41.91	-24.41/-36.5	-24.41/-36.59	-24.85/-42.7
8-9		-24.85/-45.63	-24.64/-36.34	-24.64/-36.32	-24.85/-45.35
9-10		-24.76/-51.39	-24.86/-36.11	-24.86/-35.98	-24.75/-50.21
10-11		-24.58/-58.04	-25.07/-35.19	-25.07/-36.08	-24.60/-58.6
11-12		-24.44/-68.98	-25.29/-35.19	-25.29/-36.08	-24.44/-70.46
12-13		-24.30/-85.04	-25.50/-35.05	-25.51/-36.24	-24.30/-85.83

Table 7. Summary of the maximum static and dynamic stresses obtained in each of the 16 zones shown in Figure 7.

Depth (m)	EPS Type (Elastic limit stress, kPa)	Maximum stress during earthquake for each zone, kPa			
		Column 1	Column 2	Column 3	Column 4
9-10	EPS 22 (50)	-51.39	-44.06	-44.90	-50.21
10-11		-58.04	-44.20	-44.90	-58.6
11-12		-68.98	-44.20	-43.70	-70.46
12-13		-85.04	-42.85	-43.46	-85.83

Table 8. EPS types with elastic limit stresses that exceed the estimated dynamic and static stresses.

Depth (m)	EPS Type (Elastic limit stress, kPa)	Maximum stress during earthquake for each zone, kPa			
		Column 1	Column 2	Column 3	Column 4
9-10	EPS 29 (75)	-51.39	-44.06	-44.90	-50.21
10-11		-58.04	-44.20	-44.90	-58.6
11-12		-68.98	-44.20	-43.70	-70.46
12-13	EPS 39 (103)	-85.04	-42.85	-43.46	-85.83

Table 9. Ratio in percent of the stress at 2% strain to 10% strain of various EPS types based on monotonic uniaxial tests conducted by Bartlett and Neupane (2017).

EPS type	Density	Monotonic axial strain	Young's modulus	Static deviator stress	$\dfrac{Stress\ at\ 2\%\ strain}{Stress\ at\ 10\%\ strain} \times 100$
	(kg/m^3)	(%)	(kPa)	(kPa)	(%)
EPS 15	14.8	1	3242	32	75.8
		1.5		43	
		1.75		47	
		2		50	
		5		62	
		10		66	
EPS 19	20.2	1	4747	47	76.3
		1.5		64	
		1.75		70	
		2		74	
		5		90	
		10		97	
EPS 25	25.1	1	7223	72	83.9
		1.5		99	
		1.75		109	
		2		115	
		5		131	
		10		137	
EPS 29	34.1	1	10778	108	85.8
		1.5		152	
		1.75		169	
		2		182	
		5		205	
		10		212	
EPS 39	40.1	1	13779	138	87.7
		1.5		196	
		1.75		215	
		2		228	
		5		253	
		10		260	

Table 10. Comparison of EPS compressive resistance at 2% strain with maximum static and dynamic stresses obtained in each of the 16 zones shown in Figure 7.

Depth (m)	EPS Type (Compressive resistance at 2% strain, kPa)	Maximum stress during earthquake for each zone, kPa			
		Column 1	Column 2	Column 3	Column 4
9-10		-51.39	-44.06	-44.90	-50.21
10-11	EPS 22	-58.04	-44.20	-44.90	-58.6
11-12	(103)	-68.98	-44.20	-43.70	-70.46
12-13		-85.04	-42.85	-43.46	-85.83

Table 11. Horizontal displacement results (sliding evaluation).

Sliding Between	Maximum relative X-displacement		Cumulative X-displacement[a]		Anticipated Cumulative Displacement (ACD) after earthquake[b]	
	(cm)		(cm)		(cm)	
	Left side	Middle	Left side	Middle	Left side	Middle
EPS Layer 1/EPS Layer 2	1.96	-0.82	1.96	-0.82	0.97	-0.22
EPS Layer 2/EPS Layer 3	-1.51	-0.94	0.45	-1.76	0.56	-0.28
EPS Layer 3/EPS Layer 4	-1.36	-0.95	-0.91	-2.71	-0.30	-0.21
EPS Layer 4/EPS Layer 5	-1.28	-0.98	-2.19	-3.69	-0.22	-0.17
EPS Layer 5/EPS Layer 6	-1.20	-1.01	-3.39	-4.70	-0.25	-0.12
EPS Layer 6/EPS Layer 7	-1.13	-1.04	-4.52	-5.74	-0.18	-0.06
EPS Layer 7/EPS Layer 8	-1.06	-1.08	-5.58	-6.82	-0.19	-0.02
EPS Layer 8/EPS Layer 9	-0.95	-1.11	-6.53	-7.93	-0.18	0.02
EPS Layer 9/EPS Layer 10	-0.74	-0.68	-7.27	-8.61	-0.10	0.04
EPS Layer 10/EPS Layer 11	-0.69	-0.70	-7.96	-9.31	-0.07	0.04
EPS Layer 11/EPS Layer 12	-0.64	-0.72	-8.60	-10.02	-0.05	0.04
EPS Layer 12/ Top of pavement	-0.99	-1.11	-9.59	-11.13	-0.01	0.09
Overall cumulative displacement at the top of the EPS			-11.00	-12.13		

[a] Cumulative X-displacement represents the overall sum of maximum relative displacements from the EPS's bottom to a given height or EPS interface level. Therefore, the cumulative X-displacement values can be assumed to be the estimated upper limit of X-displacement that can occur anytime during the earthquake.
[b] ACD is the cumulative displacement estimated at each level. Thus, the cumulative displacement at the end of the earthquake can be assumed to be the estimated lower limit of X-displacement that can occur at the end of the earthquake.

Figure Captions

Table Captions

41